Removal of Erythrosine B dye from wastewater by *Penicillium italicum*: experimental, DFT, and molecular docking studies

Serap Çetinkaya, Volkan Eyupoglu, Halil İbrahim Çetintaş, Ali Fazıl Yenidünya, Özgür Kebabcı & Burak Tüzün

Taylor & Francis
Taylor & Francis Group

Check for updates

Removal of Erythrosine B dye from wastewater by *Penicillium italicum*: experimental, DFT, and molecular docking studies

Serap Çetinkaya[a] (ID), Volkan Eyupoglu[b], Halil İbrahim Çetintaş[c] (ID), Ali Fazıl Yenidünya[a] (ID), Özgür Kebabcı[a] (ID) and Burak Tüzün[d] (ID)

[a]Department of Molecular Biology and Genetics, Science Faculty, Sivas Cumhuriyet University, Sivas, Turkey; [b]Department of Chemistry, Faculty of Science, Cankiri Karatekin University, Cankırı, Turkey; [c]Advanced Technology Research and Application Center (CUTAM), Sivas Cumhuriyet University, Sivas, Turkey; [d]Plant and Animal Production Department, Technical Sciences Vocational School of Sivas, Sivas Cumhuriyet University, Sivas, Turkey

Communicated by Ramaswamy H. Sarma

ABSTRACT

The study involved the adsorption of Erythrosine B onto the dead, dry, and unmodified *Penicillium italicum* cells and the analytical, visual, theoretical assessment of the adsorbent-adsorbate interactions. It also included desorption studies and reiterative usability of the adsorbent. The fungus was a local isolate and it was identified by partial proteomic experiment in a MALDI-TOFF mass spectrometer. Chemical features of the adsorbent surface were analysed by FT-IR and EDX. Surface topology was visualized by SEM. Isotherm parameters of the adsorption were determined by using three most frequently used models. Erythrosine B appeared to form a monolayer onto the biosorbent and some of the dye molecules could have also penetrated into the adsorbent particles. Kinetic results suggested a spontaneous and exothermic reaction taken place between the dye molecules and the biomaterial. Theoretical approach involved the determination of some of the quantum parameters as well as the toxic or drug potentials of the some of the components of the biomaterial.
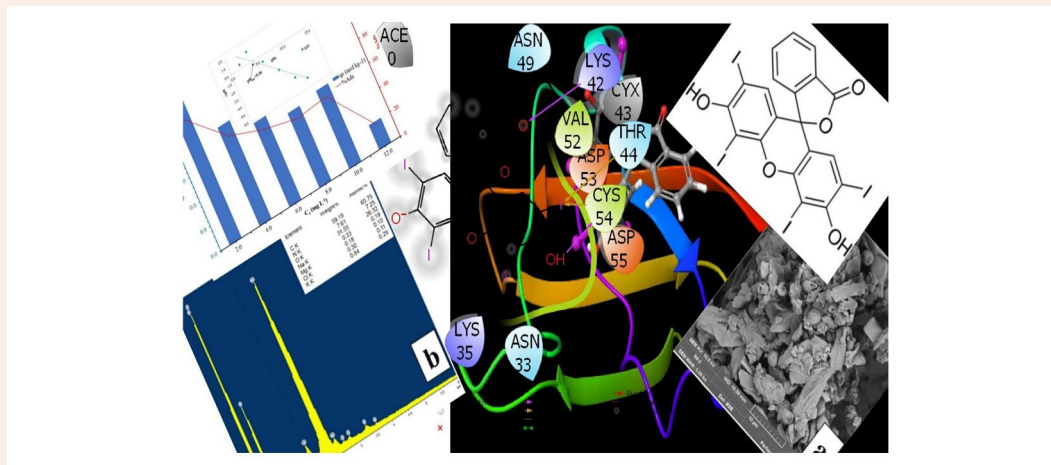
1. Introduction

Textile industry is one of the main culprits of aqueous waste as it consumes between 200 and 500 L of water per kg of a finished textile product (Singh & Khajuria, 2018; Vijayaraghavan & Yun, 2008; Waghmode et al., 2012). The water used is usually contaminated with a variety of synthetic dyes as well as surfactants, and volatile organic compounds (Balapure et al., 2015; Chen et al., 2009).

Global dye consumption in the textile sector has been estimated to be over 10,000 tons per year, and 10–15% of this amount end up in wastewater (Kunamneni et al., 2008; Pereira & Alves, 2012; Saratale et al., 2011). The release of contaminated waste into the environment not only adversely affects the appearance of the water, but also causes severe toxicity to the exposed fauna and flora species (Danouche et al., 2021; Fu & Viraraghavan, 2001).

Most frequently used methods for wastewater treatment have been flocculation, coagulation, precipitation, biosorption, membrane filtration, and electrochemical techniques (Malik & Sanyal, 2004). Among these biosorption has often been preferred as it has been relatively more effective and

less expensive. Various agricultural biomass waste has been exploited in this process: peat (Allen et al., 2004), pine bark powder (Ahmad, 2009), tomato root (Kannan et al., 2009), soybean (Mittal et al., 2010), grass, japonica, rice- and wheat bran (Wang et al., 2008), and almond shells (Atmani et al., 2009; Kumar & Ahmad, 2011). Microbial organisms also constitute a versatile source of biomass for adsorption (Wang et al., 2015). Fungal cells, for example, can easily be obtained as by-products of brewing industries (Salvi & Chattopadhyay, 2017). Studies have shown that inactive (dead and dry) fungal biomass has advantages over live biomass as it does not require the addition of nutrients. They also do not produce chemicals inhibitory to adsorption or toxic compounds detrimental for aquatic life. In addition, inanimate biomass has high storage stability and can be reused many times as it allows easy elution of adsorbed materials (Souza et al., 2020). In recent years, the adsorption method has been tried to remove some hazardous substances (Kamal et al., 2020, 2022).

Various studies have focused on the biosorption of dyes with microorganisms such as algae (Aksu & Tezer, 2005), fungi (O'Mahony et al., 2002), bacteria (Hu, 1996) and yeasts (Aksu & Dönmez, 2003). Among them, mould biomass is envisaged as the most efficient and least expensive biosorbent (Fu & Viraraghavan, 2001; Maurya et al., 2006; Saeed et al., 2009; Vijayaraghavan et al., 2008). Both macro- and micro fungi have also been used as biosorbent: *Trametes versicolor* (Bayramoğlu et al., 2006), *Ganoderma applanatum* (Matos et al., 2007), *Funalia trogii* (Yesilada et al., 2002), *Rhizopus* (Zeroual et al., 2006), *Aspergillus flavus* (Gajera et al., 2015), *Aspergillus niger* (Fu & Viraraghavan, 2002), and *Penicillium fellutinum* (composite with bentonite) (Bouras et al., 2017; Rashid et al., 2016).

Due to their potential toxicity and carcinogenic effects, dyes have been the subjects of a wide variety of environmental studies (Dotto & Pinto, 2011). Erythrosine B (C.I 45430) is a water-soluble anionic xanthene dye (Figure 1) and widely used especially in the food, cosmetic, and pharmaceutical industries (Al-Degs et al., 2012; Sharifzade et al., 2017). It is a widely used industrial dye and appears to have some serious toxic properties as it has been evidenced to cause allergic reactions in the eyes, irritation of the skin and upper respiratory tract, severe headaches, nausea, water-
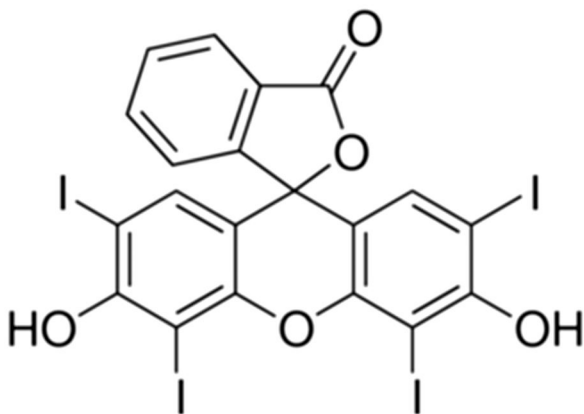
borne diseases such as dermatitis. What is more, free iodine, which is released by the degradation of this dye compound in nature, may adversely affect thyroid functions and can be an agent of atopic diseases (Salvi, 2018; Uysal & Aral, 1998).

In this study, the efficacy of a new biosorbent prepared from inanimate *Penicillium italicum* in removing Erythrosine B, was investigated. To enable the process to be economical, the fungus was not chemically modified and fed on low-cost nutrients. The research basically involved kinetic, isothermic, and thermodynamic analyses of the adsorption. Desorption studies were also carried out. Some computational analyses, using Gaussian09 RevD.01 and GaussView 6.0 (Dennington et al., 2016; Frisch et al., 2009) and B3LYP, HF, and M06-2x (Becke, 1992; Hohenstein et al., 2008; Vautherin & Brink, 1972) programs, have been performed to assess both the chemical and biological activities of molecules. In order to calculate the biological activity of after molecules, their activity against the crystal structure of Penicillium proteins (PDB ID: 2NC2 (Huber et al., 2018) and 2NB0 (Holzknecht et al., 2022)) was calculated. Finally, ADME/T calculations were made to examine the drug ability of the adsorbent material.

2. Materials and methods

2.1. Preparation of biosorbent

Penicillium italicum was isolated from an artisanal yogurt sample using PDA (potato dextrose broth: 15 g bacteriological agar, 20 g dextrose and 4 g potato starch in g/L, pH 5.6) for 5 d at 30 °C. Biomass for adsorption was prepared in 300 ml PDA for 7d incubation at 30 °C at 150 rpm. The culture was centrifuged at 7,200 rpm for 10 min (Vimont et al., 2019).

2.2. Identification by mass spectrometry

Partial protein homology by MALDI-TOFF Mass Spectrometry (Bruker IVD MALDI Biotyper, Sivas Cumhuriyet University Hospital) identified the yoghurt mould to be *Penicillium italicum*.

2.3. Characterization of the biosorbent

Dead and dry *Penicillium italicum*, biosorbent, was analysed by Fourier Transform Infrared (FTIR) Spectrometry (ATR, Bruker, Tensor II), Scanning Electron Microscope (SEM), Energy Dissipative X-Ray (EDX) at CUTAM Central Laboratory (Sivas Cumhuriyet University, Turkey), and by ultraviolet-visible Spectroscopy (TESCAN MIRA3 XMU, T-60, China).

2.4. Effect of PZC on the biosorbent

To determine the PZC values of biosorbent, the pH of 0.1 mol L^{-1} KNO$_3$ solution was adjusted in the range between 1.0 and 12.0, using HCl or NaOH (0.1 mol L^{-1}). Biosorbent, 0.1 g, of was added. Initial pH values were plotted against ΔpH to obtain PZC (Smiciklas et al., 2008), and final pH values were read after 24 h.

Figure 1. Chemical structure of Erythrosine B dye.

2.5. Experimental design and biosorption tests

Biosorption reactions were carried out for 24 h at 25 °C in 10 mL final reaction samples at pH 7.15, including 50 mg biosorbent and 500 mg L^{-1} Erythrosine B. Using dye concentrations between 10 and 1000 mg L^{-1}, the optimum dye retaining capacity was found to be 500 mgL^{-1}. Samples were then centrifuged (3500 rpm, 10 min). Erythrosine B remaining in the solution was determined at 525 nm by UV-Vis spectrophotometry (Çetinkaya et al., 2022; Salvi, 2018). Experiments were repeated thrice, controls (without biosorbent) were performed in parallel. Adsorption percentage, Q (mol kg$_{-1}$), and % desorption ARE calculated by Equations (1)–(3).

$$\text{Adsorption\%} = \left[\frac{C_i - C_f}{C_i}\right] x100 \tag{1]}$$

$$Q = \left[\frac{C_i - C_f}{m}\right] xV \tag{2}$$

$$\text{Desorption\%} = \frac{Q_{des}}{Q_{ads}} x100 \tag{3}$$

where C_i, initial dye concentration (mg L^{-1}); C_f, dye concentration (mg L^{-1}) at time t; m, dry biosorbent (g); V, reaction volume (L); Q_{ads}, dye adsorbed (mol kg^{-1}); and Q_{des}, desorbed dye (mol kg^{-1}).

2.6. Isotherms of adsorption

The equations below were used for the isotherm calculations (Baybaş & Ulusoy, 2011):

$$Q = \frac{X_L K_L C_e}{1 + K_L C_e} \tag{4}$$

$$Q = K_F C_e^\beta \tag{5}$$

$$Q = Q_{DR} e^{-K_{DR}\varepsilon^2} \tag{6}$$

$$\varepsilon = RTln\left(1 + \frac{1}{C_e}\right) \tag{7}$$

$$E_{DR} = (2K_{DR})^{-0.5} \tag{8}$$

where Q (mol kg^{-1}), adsorbed material B; K_L, isotherm parameters; C_e, the equilibrium concentration (mol L^{-1}); X_L (mol kg^{-1}), maximum adsorbent capacity; K_F, Freundlich constant; β, biosorbent surface heterogeneity; X_{DR}, a measure of adsorption capacity; R, the ideal gas constant (8.314 Jmol^{-1}K^{-1}); T, the absolute temperature (K); K_{DR}, the activity coefficient (mol^{2}KJ^2); ε, the Polanyi potential.

2.7. Calculation of the adsorption kinetics

Adsorption kinetics were determined by three commonly used models: (PFO), pseudo-second-order (PSO) and intraparticle diffusion (IPD) (Baybaş & Ulusoy, 2011) (Equations 9–11).

$$Q_t = Q_e[1 - e^{-k_1 t}] \tag{9}$$

$$Q_t = \frac{t}{\left[\frac{1}{k_2 Q_e^2}\right] + \left[\frac{t}{Q_e}\right]} \tag{10}$$

$$Q_t = k_i t^{0.5} \tag{11}$$

where Q_t (mol kg^{-1}), adsorbed dye; t, (min) time; Q_e (mol kg^{-1}), adsorption at equilibrium; k_1, k_2; k_i, the rate constants of the PFO (min^{-1}); PSO (mol^{-1}kg min^{-1} IPD (mol^{-1}kg min$^{-0.5}$).

2.8. Thermodynamics of adsorption

The parameters ΔH^0 (enthalpy), ΔS^0 (entropy), and ΔG^0 (Gibbs free energy) were calculated (Equations 12–15), and these thermodynamic parameters were used to see if the adsorption process was spontaneous (Şimşek et al., 2022).

$$K_D = \frac{Q}{C_e} \tag{12}$$

$$\Delta G^0 = -RTlnK_D \tag{13}$$

$$lnK_D = \frac{\Delta S^0}{R} - \frac{\Delta H^0}{RT} \tag{14}$$

$$\Delta G^0 = \Delta H^0 - T\Delta S^0 \tag{15}$$

2.9. Theoretical methods

Using Gaussian09 RevD.01 and GaussView 6.0 programs (Dennington et al., 2016; Frisch et al., 2009) and B3LYP, HF, and M06-2x methods (3-21 g, lanl2dz, and STO-3G) a number of quantum parameters [HOMO (Highest Occupied Molecular Orbital), LUMO (Lowest Unoccupied Molecular Orbital), ΔE (HOMO-LUMO energy gap), chemical potential (μ), electrophilicity (ω), chemical hardness (η), and global softness (σ)] were determined and nucleophilicity (ε), dipole moment, and energy value were defined (Lakhrissi et al., 2022; Mermer et al., 2022).

$$\chi = -\left(\frac{\partial E}{\partial N}\right)_{\upsilon(r)} = \frac{1}{2}(I + A) \cong -\frac{1}{2}(E_{HOMO} + E_{LUMO}) \tag{16}$$

$$\eta = -\left(\frac{\partial^2 E}{\partial N^2}\right)_{\upsilon(r)} = \frac{1}{2}(I - A) \cong -\frac{1}{2}(E_{HOMO} - E_{LUMO}) \tag{17}$$

$$\sigma = 1/\eta \quad \omega = \chi^2/2\eta \quad \varepsilon = 1/\omega \tag{18}$$

After the molecules were optimized by Gaussian software, they were used for calculations in LigPrep module (Schrödinger Release 2021-3,3, 2021a). The Glide ligand docking module (Al-Janabi et al., 2022) was then used to examine the interactions between the molecules. Maestro Molecular modeling platform (version 12.8) was used for molecular docking calculations (Schrödinger Release 2019-4,4, 2019; Schrödinger Release 2021-3,3, 2021b). Calculations were made using the OPLS4 method in all calculations. Lastly, ADME/T (absorption, distribution, metabolism, excretion and toxicity) was assessed to gain some insight into drug potential of the studied molecules. The Qik-prop module (Schrödinger Release 2021-3,3, 2021c) predicted the possible effects of the molecules in human metabolism.
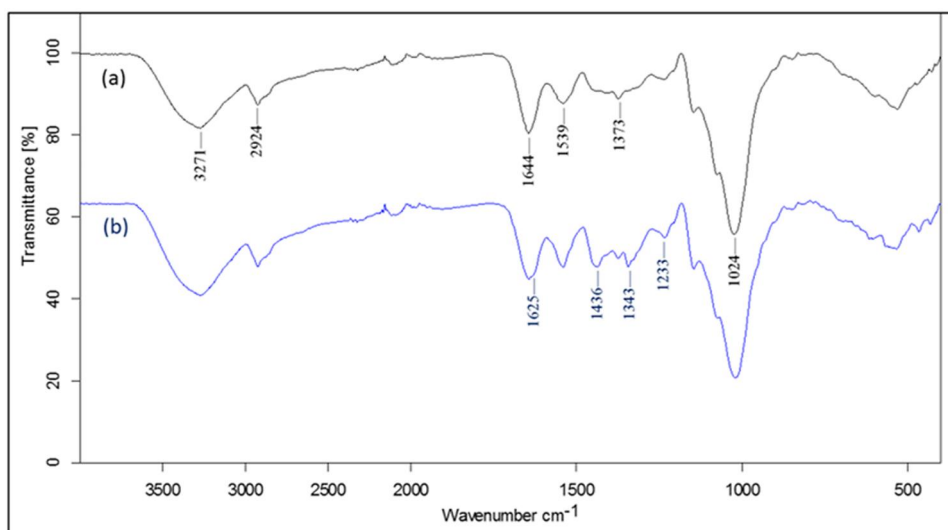
Figure 2. FT-IR spectra of *Penicillium italicum* before (a) and after (b) the biosorption of Erythrosine B.

3. Results and discussion

3.1. FTIR analysis

FTIR analysis of *Penicillium italicum* was carried out and the adsorption bands corresponding to various functional groups of important macromolecules such as carbohydrates, lipids, nucleic acids and proteins were defined and shown in Figure 2. The FT-IR spectra of untreated fungus presented a characteristic band at $3271 \, cm^{-1}$ due to N-H stretching vibrations from the proteins. The peak at $2924 \, cm^{-1}$ corresponded to symmetric stretching vibrations C-H bonds of lipids (Lecellier et al., 2015; Lozano et al., 2017). The adsorption bands located at $1644 \, cm^{-1}$ and $1539 \, cm^{-1}$ were assigned to $C = O$ stretching vibration of amide I and a mixture of N-H bending and C-H stretching vibrations of amide II, respectively. These bonds were related to CH_3 and CH_2 groups in proteins and fatty acids (Kamnev, 2013; Ye et al., 2017). The band at $1373 \, cm^{-1}$ was associated with $-COO^-$ symmetric stretching vibrations of carboxyl groups and amino acid side chains (Lozano et al., 2017). C-O stretching peak due to carbohydrates was observed at $1024 \, cm^{-1}$ (Al Mousawi & Razaq, 2021). After treatment of *P. italicum* with the dye, some new peaks identical to Erythrosine B appeared in the FTIR spectra. These peaks were benzene ring stretching vibration appearing as a shoulder at $1625 \, cm^{-1}$, $-COO^-$ symmetric stretching vibration at $1436 \, cm^{-1}$ and stretching vibrations due to C-H in-plane deformation of xanthene ring at $1343 \, cm^{-1}$ and $1233 \, cm^{-1}$ (Kaur & Datta, 2013; Tonglairoum et al., 2017). Thus, the presence of Erythrosine B molecules on the adsorbent was confirmed by the FT-IR analysis.

3.2. SEM-EDX analysis

To examine the morphological alterations of *Penicillium italicum*, SEM analysis was carried out before and after adsorption. The ultrastructure of the fungus consisted of flat and tubular shaped hyphae in accord with the usual morphology of *P. italicum* (Che et al., 2019; Li et al., 2021) (Figure 3a). The cell walls were covered with the dye molecules after the treatment (Figure 3c). This finding was confirmed by EDX analyses. After the adsorption process, 1.18% (w%) iodine content due to Erythrosine B was determined in the dye-treated samples (Figure 3b–d).

3.3. Effect of pH

Adsorption of Erythrosine B onto the dead biomass of *Penicillium italicum* was significantly efficient, 99%, at pH 2 (Figure 4). Reactive hydroxyl-, ether-, and carbonyl groups in Erythrosin B could have played a determining role in the pH behaviour of adsorption. Low pH may be involved in the protonation of the nitrogen atoms of the biomass. Between these groups and atoms electrostatic attraction, van der Waals, dispersion forces, hydrogen bond, ion-dipole might have taken place.

The surface charge of the adsorbent, 5.39, could be another important factor contributing to the efficiency of adsorption (Figure 4). This value could indicate that the surface of the mould was positive at acidic pH as the hydronium ions might have protonated all nitrogen atoms inside the biomass particles, resulting in a vertical increase of adsorption.

3.4. Quantity of the adsorbent

The effect of adsorbent quantity on the adsorption of Erythrosine B was studied between 30 and 250 mg and it was compared with those found in the literature (Table 1) (Figure 5). The maximum adsorption, 91.71%, was obtained with 100 mg adsorbent and Q_e values decreased by increasing the adsorbent amount.

3.5. Modelling of adsorption process

Experimental results were evaluated by using three kinetic models (Figure 6), and the related linear and non-linear isotherm parameters were presented (Table 2). The highest R^2
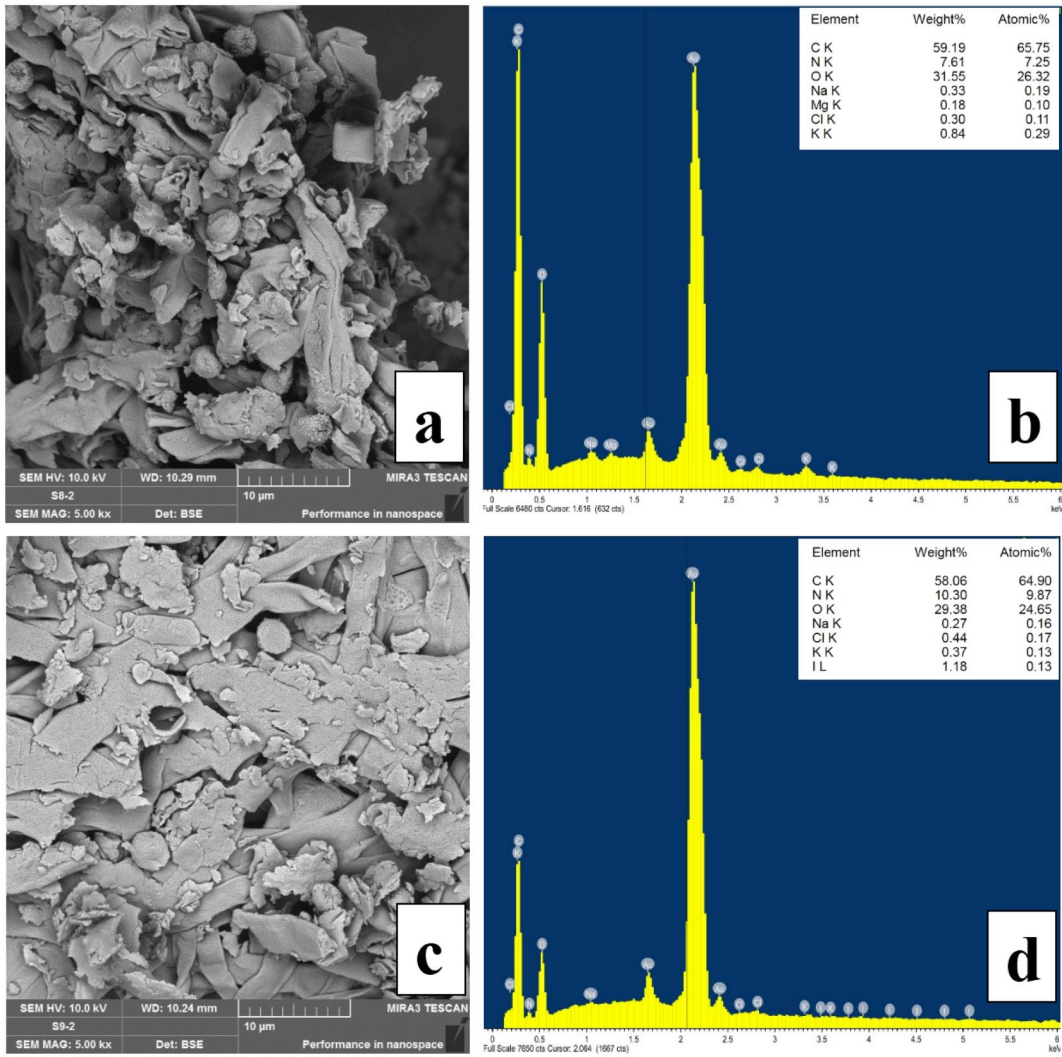
Figure 3. SEM-EDX analyses of *Penicillium italicum* before (a,b) and after (c,d) adsorption.
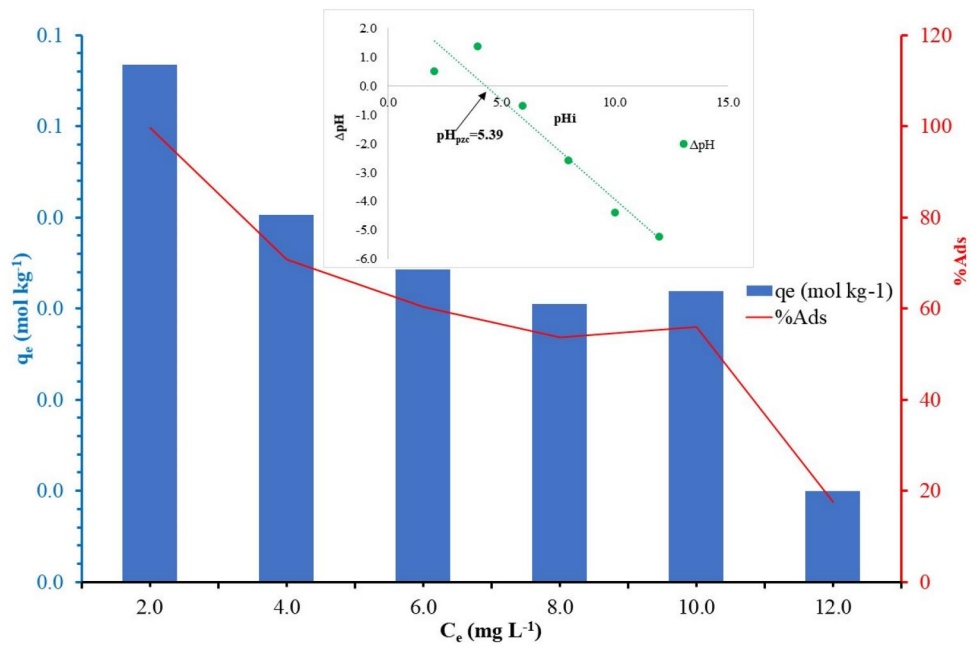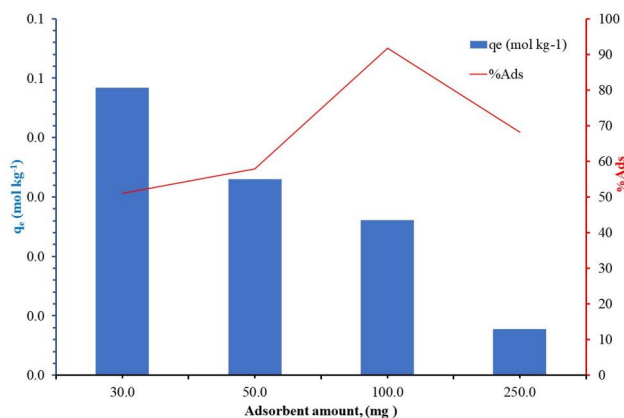

Figure 4. pH dependency of the adsorption.

Table 1. Results from literature on biosorption of various dyes.

Biosorbent used	Dye	Biosorption capacities (mg/g) or Removal efficiency (%)	References
Raphia hookeri	Erythrosine B	87.78%	(Okoye et al., 2019)
Aspergüllus niger	Basic Blue 9	18.5 mg/g	(Fu & Viraraghavan, 2000)
Candida sp.	Remazol Blue	169 mg/g	(Aksu & Dönmez, 2003)
Rhizopus arrhizus	Erythrosine B	363.6 mg/g	(Salvi, 2018)
Spirulina platensi	Congo Red	82.6%	(Nautiyal et al., 2016)
Penicillium italicum	Erythrosine B	91.71%	(Current study)

Figure 5. Adsorbent dependency of adsorption.
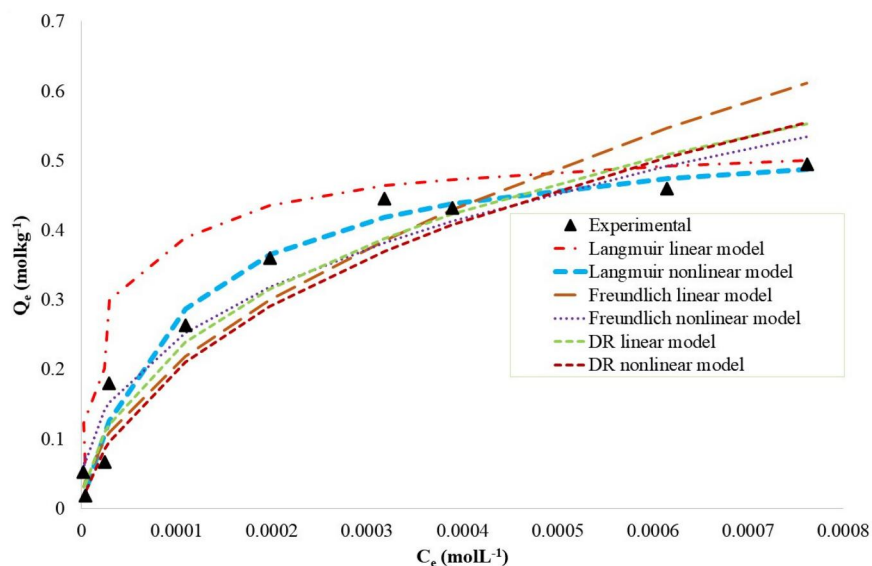
Figure 6. Experimental adsorption isotherms and their compatibility with the Langmuir-, Freundlich-, and D-R models.

Table 2. Isotherm models parameters.

	Langmuir parameters		R2	Freundlich parameters		R2	D-R parameters		R2
Linear	X_L (mg g^{-1})	0.550	0.975	β	1.889	0.880	K_{DR} (mol^{2}kJ^{-2})*10^9	4.326	0.883
	K_L (Lmg^{-1})	9985.279		X_F	27.364		Q_{DR} (mol g^{-1})	2.173	
							ε kjmol^{-1}	10.751	
Nonlinear	X_L (mg g^{-1})	0.551	0.977	β	2.590	0.941	K_{DR} (mol^{2}kJ^{-2})*10^9	5.000	0.909
	K_L (Lmg^{-1})	9898.622		X_F	8.551		Q_{DR} (mol g^{-1})	2.700	
							ε kjmol^{-1}	10.000	

values were better fitted to the Langmuir model (R^2=0.977), pointing to the occurrence of a monolayer adsorption. The maximum adsorption capacity (X_L) and the Langmuir constant (K_L) values were found as 0.55 mol kg^{-1} and 9898.622 L mol^{-1}, respectively. The adsorption capacity (X_F) and surface heterogeneity of adsorbent (β) for Freundlich models were found to be 8.551 and 2.590 respectively and implied that reaction conditions were appropriate. The adsorption appeared to be physical because the adsorption energy (ε) was approximately 10 kJ mol^{-1}.
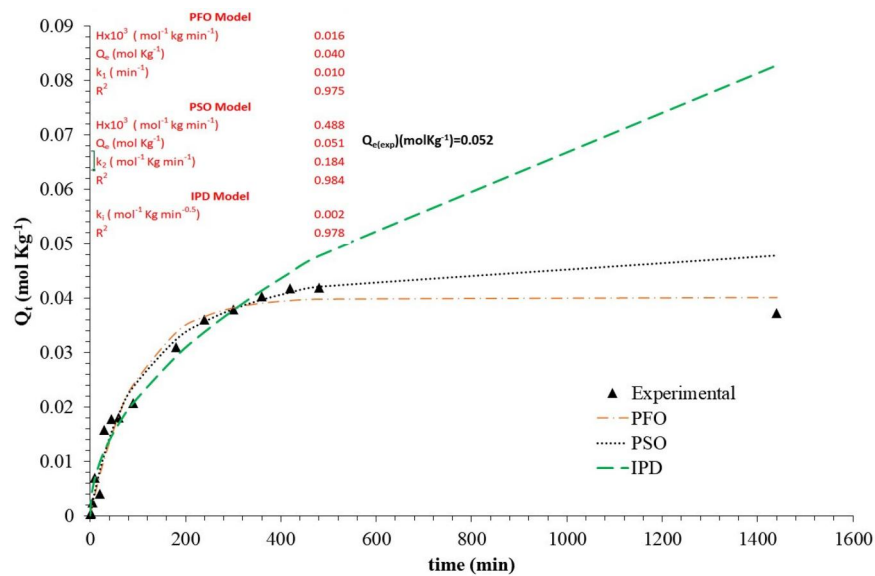
Figure 7. Compatibility of the adsorption kinetics with the PFO, PSO and IPD models.

Table 3. Energetics of the adsorption.

Temp	KD	ΔG^0	ΔH^0	ΔS^0
K	LKg^{-1}	KJmol^{-1}	KJmol^{-1}	Jmol^{-1}K^{-1}
278.15	3443.58	−24.16	4.56	86.86
298.15	12549.48	−25.89		
313.15	3635.47	−27.20		
	Average ΔG^0	−25.75		
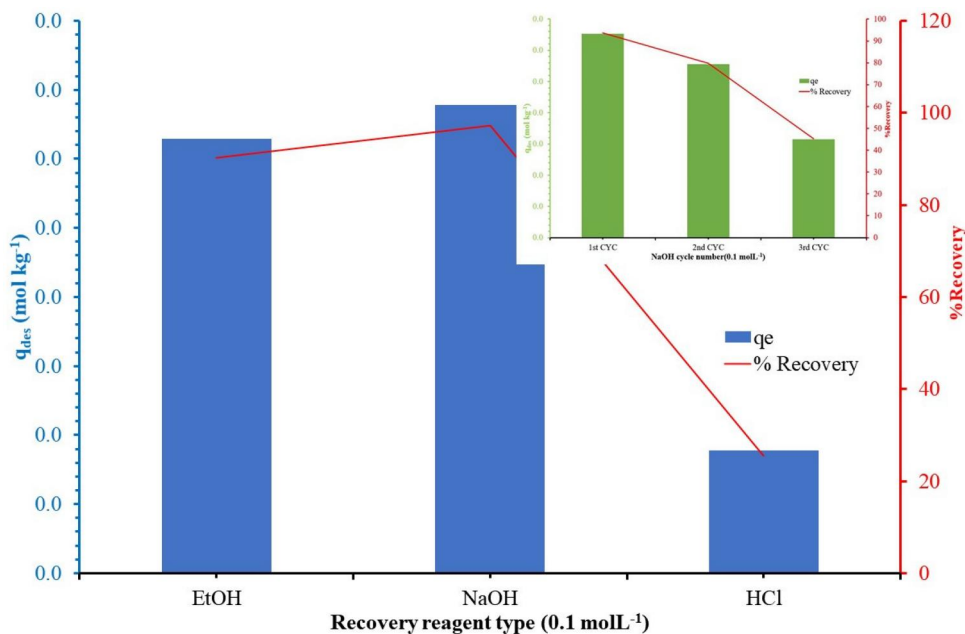
Figure 8. The efficiency of recovery.

3.6. Effect of incubation time

Application of the PFO, PSO, and IPD models confirmed that the adsorption rate was expectedly faster at the beginning (Figure 7). The saturation plateau appeared between 480th min and 1440th min. R^2 values were concordant with those of the PSO model and with the theoretical Q_e (0.051) and experimental Q_e (0.052) findings. The results of the IPD

model argued that some Erythrosine B molecules might have penetrated into the adsorbent particles (Çetinkaya et al., 2022).

ΔH^0 of the adsorption, 4.56 KJmol^{-1} suggested an endothermic, and the adsorption entropy, 86.86 Jmol^{-1} K^{-1}, implied a random binding feature of Erythrosine B. The Gibbs free energy values were −24.16 kJ mol^{-1}, −25.89 kJ

Table 4. The calculated quantum chemical parameters of molecules.

| E$_{HOMO}$	E$_{LUMO}$	I	A	ΔE	η	μ	χ	Pİ	ω	ε	dipol	Energy
B3LYP/3-21g level												
−0.9124	−0.7007	0.912	0.7007	0.2117	0.1059	9.447	0.806	−0.8066	3.0728	0.3254	4.1213	−780941.7670
B3LYP/STO-3G level												
1.8547	1.9494	−1.854	−1.9494	0.0947	0.0473	21.120	−1.902	1.9021	38.205	0.0262	3.6186	−776610.0340
B3LYP/LANL2DZ level												
−6.5175	−2.1647	6.517	2.1647	4.3528	2.1764	0.459	4.341	−4.3411	4.3294	0.2310	6.2374	−32333.7328
HF/3-21g level												
2.6809	3.1250	−2.680	−3.1250	0.4441	0.2220	4.503	−2.902	2.9029	18.975	0.0527	4.4668	−780461.0794
HF/STO-3G level												
6.6372	6.6859	−6.637	−6.6859	0.0487	0.0244	41.060	−6.661	6.6615	911.04	0.0011	3.4986	−776199.6793
HF/LANL2DZ level												
−8.9298	1.3872	8.929	−1.3872	10.3170	5.1585	0.193	3.771	−3.7713	1.3785	0.7254	5.3550	−32120.9852
M062X/3-21g level												
−0.0218	0.2664	0.021	−0.2664	0.2882	0.1441	6.940	−0.122	0.1223	0.0519	19.261	4.1020	−780971.3880
M062X/STO-3G level												
3.1677	3.3658	−3.167	−3.3658	0.1981	0.0991	10.095	−3.266	3.2668	53.870	0.0186	3.6747	−776639.0727
M062X/LANL2DZ level												
−7.7080	−1.2444	7.708	1.2444	6.4636	3.2318	0.3094	4.476	−4.4762	3.0999	0.3226	6.2814	−32318.2090

Erythrosin   HOMO   LUMO   ESP
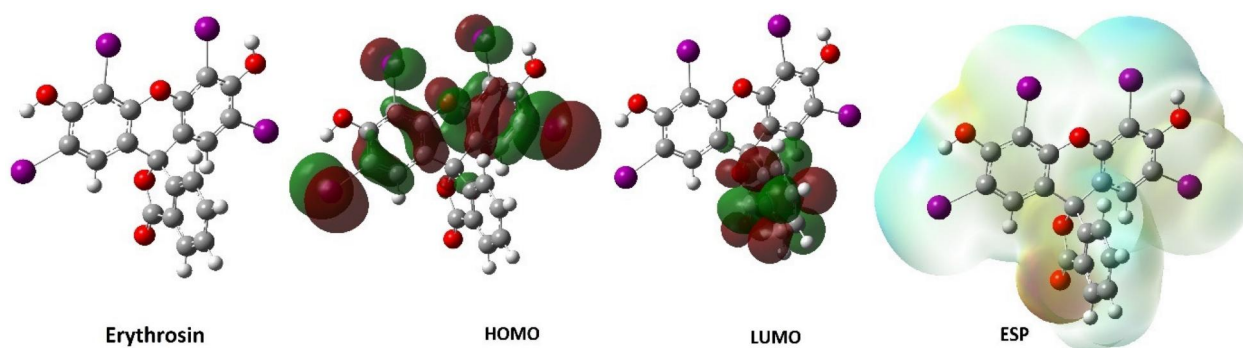
Figure 9. Optimized HOMO, LUMO, and ESP structures. Regions of high electron density were indicated in red.
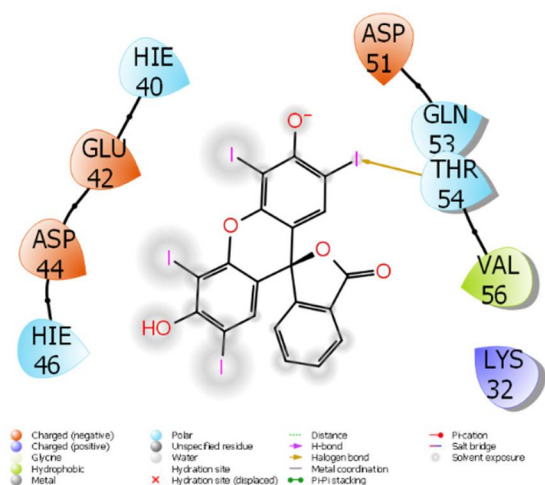
Figure 10. Presentation interactions of molecule with **2NC2**.

mol^{-1}, and −27.20 kJ mol^{-1} for 278.15, 298.15, and 313.15 K respectively, and their average value, −25.75 kJ mol^{-1}, indicated a temperature dependent but spontaneous course of adsorption (Table 3).

adsorption/desorption cycles, the adsorbent still retained approximately 45% of its adsorption capacity. Electron micrographs did not reveal significant topological adsorbent deformations after the three repeats of desorption.

3.7. Desorption and recovery

The desorption efficiency of the elution solutions used were NaOH > EtOH > HCl (Figure 8). After three

3.8. Computational study

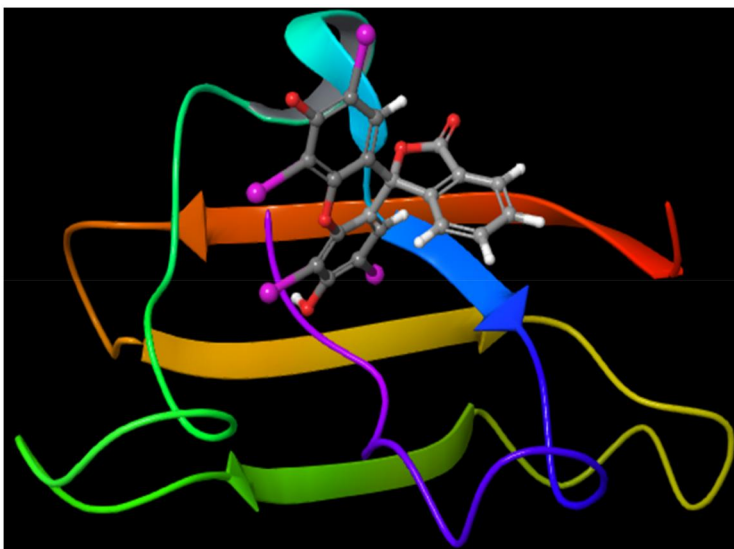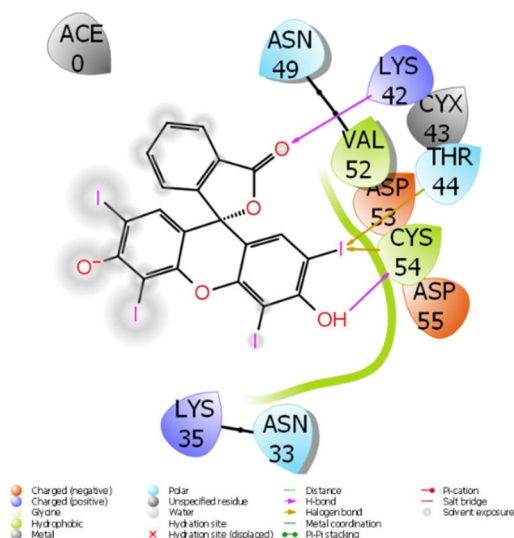Theoretical calculations compared the chemical and biological activities of the mould adsorbent. Many quantum

Figure 11. Presentation interactions of molecule with **2NB0**.

Table 5. Numerical values of the docking parameters of molecule against proteins.

	2NC2	7U0N
Docking score	−2.99	−2.92
Glide ligand efficiency	−0.10	−0.10
Glide hbond	0.00	−0.47
Glide evdw	−38.30	−25.13
Glide ecoul	2.24	−10.67
Glide emodel	−43.14	−44.78
Glide energy	−36.06	−35.80
Glide einternal	0.00	0.45
Glide posenum	128	120

Table 6. ADME properties of molecule.

Parameters	Erythrosine B	Referance range
mol_MW	836	130–725
dipole (D)	6.3	1.0–12.5
SASA	653	300–1000
FOSA	0	0–750
FISA	142	7–330
PISA	227	0–450
WPSA	285	0–175
volume (A^3)	1188	500–2000
donorHB	2	0–6
accptHB	5	2.0–20.0
glob (Sphere =1)	0.8	0.75–0.95
QPpolrz (A^3)	42.3	13.0–70.0
QPlogPC16	14.3	4.0–18.0
QPlogPoct	21.6	8.0–35.0
QPlogPw	11.3	4.0–45.0
QPlogPo/w	4.9	−2.0–6.5
QPlogS	−7.2	−6.5–0.5
ClQPlogS	−15.6	−6.5–0.5
QPlogHERG	−5.4	*
QPPCaco (nm/sec)	451	**
QPlogBB	−0.2	−3.0–1.2
QPPMDCK (nm/sec)	7574	**
QPlogKp	−3.1	Kp in cm/hr
IP (ev)	8.9	7.9–10.5
EA (eV)	1.5	−0.9–1.7
#metab	2	1–8
QPlogKhsa	0.7	−1.5–1.5
Human Oral Absorption	1	–
Percent Human Oral Absorption	90	***
PSA	88	7–200
RuleOfFive	1	Maximum is 4
RuleOfThree	1	Maximum is 3
Jm	0.00004	-

Note: *below -5, **<25 is poor and >500 is great, *** <25% is poor and >80% is high.

chemical parameters and each of the quantum chemical parameters elucidated different properties of the adsorbent components. Two of the most important parameters, HOMO and LUMO, predicted the ability of molecules to donate and accept electrons (Bhat et al., 2022). Energy gap, ΔE, findings helped explain the energetics of the active adsorbent components. The smallest difference between HOMO and LUMO energy values indicated the highest activity (Rezaeivala et al., 2022).

Apart from these parameters in Table 4, there are parameters that explain many chemical properties of molecules. Electronegativity, as another significant parameter, measures the attraction strength of bond electrons by the adsorbent atoms. High electronegativity indicates high attraction strengths (Bhat et al., 2022). Chemical hardness and softness, on the other hand, provides information on the group reactivity and stability (Rezaeivala et al., 2022). Soft molecules are considered relatively more reactive as they can readily donate electrons.

Although many parameters are calculated as a result of the calculations, only a few parameters are visualized. These images are given in Figure 9, in this way the optimized structures of the molecules include HOMO, LUMO, and the representation of the electrostatic potentials of the molecules. Electrostatic potentials of molecules give information about electron density. Although the red colored regions are high

in electron density, the blue colored regions are electron poor (Yalazan et al., 2022).

After examining the DFT properties of molecules, it is important to compare the activity against biological materials to achieve better and more reliable results. In the study, the most important of many factors affecting the results obtained against proteins to compare the activities of molecules is the chemical interaction that occurs between

proteins and molecules. These chemical interactions that occur are shown in Figures 10–11.

Molecular docking results (Table 5) indicated interactions between the protein molecules of the biomaterial (Glide hbond, Glide evdw, and Glide ecoul) (Kafa et al., 2022), while the remaining parameters showed the chemical interactions occurred between proteins and other molecules (Glide emodel, Glide energy, Glide einternal, and Glide posenum) (Taslimi et al., 2022).

ADME/T evaluated the potential toxicity of the biomaterial (Table 6). This analysis made use of the molar mass (mol_ MW), dipole moment (dipole), total solvent accessible surface area (SASA), (v/v), number of hydrogens (donorHB and accptHB), globularity descriptor (glob), and predicted polarizability (QPpolrz) values (Poustforoosh et al., 2022). In addition, IC50 value for blockage of HERG K^+ channels (QPlogHERG), apparent Caco-2 cell permeability (QPPCaco), and brain/blood partition coefficient (QPlogBB) were predicted (Tokalı et al., 2022).

4. Conclusions

The initial pH (2.0) of the medium significantly affected the sorption capacity of dry moulds. The adsorption results indicated that a monolayer adsorption had occurred and these were in agreement with the Langmuir model. Experimental data were also proven to be compatible with the PSO model.

The presence of Erythrosine B molecules on the adsorbent was confirmed by FT-IR and SEM analyses. These two approaches clearly indicated that the surface of the cells was covered with dye molecules. In addition, the data obtained from the EDX were also consistent with these results. These results together showed that dry mould could retain textile dyes at meaningful ratios.

Acknowledgments

Disclosure statement

The authors declare that they do not have any competing interests to disclose.

Funding

ORCID

Serap Çetinkaya 🔟 http://orcid.org/0000-0001-7372-1704
Halil İbrahim Çetintaş 🔟 http://orcid.org/0000-0003-1769-0098
Ali Fazıl Yenidünya 🔟 http://orcid.org/0000-0002-9886-977X
Özgür Kebabcı 🔟 http://orcid.org/0000-0002-9404-747X
Burak Tüzün 🔟 http://orcid.org/0000-0002-0420-2043

Author's contributions

Serap Çetinkaya: investigation, data curation, formal analysis, writing–review & editing. Volkan Eyupoglu: conceptualization, methodology, writing–review & editing. Halil İbrahim Çetintaş: investigation, writing–review & editing. Ali Fazıl Yenidünya: conceptualization, supervision, writing–review & editing. Özgür Kebabcı: investigation, formal analysis. Burak Tüzün: supervision, validation, writing–review & editing.

References

Ahmad, R. (2009). Studies on adsorption of crystal violet dye from aqueous solution onto coniferous pinus bark powder (CPBP). *Journal of Hazardous Materials*, *171*(1–3), 767–773. https://doi.org/10.1016/j.jhazmat.2009.06.060

Al-Degs, Y. S., Abu-El-Halawa, R., & Abu-Alrub, S. S. (2012). Analyzing adsorption data of erythrosine dye using principal component analysis. *Chemical Engineering Journal*, *191*, 185–194. https://doi.org/10.1016/j.cej.2012.03.002

Aksu, Z., & Dönmez, G. (2003). A comparative study on the biosorption characteristics of some yeasts for Remazol Blue reactive dye. *Chemosphere*, *50*(8), 1075–1083. https://doi.org/10.1016/S0045-6535(02)00623-9

Aksu, Z., & Tezer, S. (2005). Biosorption of reactive dyes on the green alga Chlorella vulgaris. *Process Biochemistry*, *40*(3–4), 1347–1361. https://doi.org/10.1016/j.procbio.2004.06.007

Al Mousawi, H. G., & Razaq, R. A. (2021). Fermentation extract of Penicillium italicum and Fusarium oxysporum and a statement of its biological effectiveness. *Systematic Reviews in Pharmacy*, *12*, 1493–1500.

Al-Janabi, I., A. S., Yavuz, S. Ç., Köprü, S., Tapera, M., Kekeçmuhammed, H., Akkoç, S., Tüzün, B., Patat, Ş., & Sarıpınar, E. (2022). Antiproliferative activity and molecular docking studies of new 4-oxothiazolidin-5-ylidene acetate derivatives containing guanylhydrazone moiety. *Journal of Molecular Structure*, *1258*, 132627. https://doi.org/10.1016/j.molstruc.2022.132627

Allen, S. J., Mckay, G., & Porter, J. F. (2004). Adsorption isotherm models for basic dye adsorption by peat in single and binary component system. *Journal of Colloid and İnterface Science*, *280*(2), 322–333. https://doi.org/10.1016/j.jcis.2004.08.078

Atmani, F., Bensmaili, A., & Mezenner, N. Y. (2009). Synthetic textile effluent removal by skin almonds waste. *Journal of Environmental Science and Technology*, *2*(4), 153–169. https://doi.org/10.3923/jest.2009.153.169

Balapure, K., Bhatt, N., & Madamwar, D. (2015). Mineralization of reactive azo dyes present in simulated textile waste water using down flow microaerophilic fixed film bioreactor. *Bioresource Technology*, *175*, 1–7. https://doi.org/10.1016/j.biortech.2014.10.040

Baybaş, D., & Ulusoy, U. (2011). Polyacrylamide–clinoptilolite/Y-zeolite composites: characterization and adsorptive features for terbium. *Journal of Hazardous Materials*, *187*(1–3), 241–249. https://doi.org/10.1016/j.jhazmat.2011.01.014

Bayramoğlu, G., Çelik, G., & Arica, M. Y. (2006). Biosorption of reactive blue 4 dye by native and treated fungus Phanerocheate chrysosporium: Batch and continuous flow system studies. *Journal of Hazardous Materials*, *137*(3), 1689–1697. https://doi.org/10.1016/j.jhazmat.2006.05.005

Becke, A. D. (1992). Density-functional thermochemistry. I. The effect of the exchange-only gradient correction. *The Journal of Chemical Physics*, *96*(3), 2155–2160. https://doi.org/10.1063/1.462066

Bhat, M. A., Tüzün, B., Alsaif, N. A., Khan, A. A., & Naglah, A. M. (2022). Synthesis, characterization, molecular modeling against EGFR target and ADME/T analysis of novel purine derivatives of sulfonamides. *Journal of Molecular Structure*, *1257*, 132600. https://doi.org/10.1016/j.molstruc.2022.132600

Bouras, H. D., Yeddou, A. R., Bouras, N., Hellel, D., Holtz, M. D., Sabaou, N., Chergui, A., & Nadjemi, B. (2017). Biosorption of Congo red dye by Aspergillus carbonarius M333 and Penicillium glabrum Pg1: Kinetics, equilibrium and thermodynamic studies. *Journal of the Taiwan*

Institute of Chemical Engineers, 80, 915–923. https://doi.org/10.1016/j.jtice.2017.08.002

Che, J., Chen, X., Ouyang, Q., & Tao, N. (2019). p-Anisaldehyde exerts its antifungal activity against Penicillium digitatum and Penicillium italicum by disrupting the cell wall integrity and membrane permeability. *Journal of Microbiology and Biotechnology*, 30(6), 878–884. https://doi.org/10.4014/jmb.1911.11032

Chen, C. Y., Kuo, J. T., Cheng, C. Y., Huang, Y. T., Ho, I. H., & Chung, Y. C. (2009). Biological decolorization of dye solution containing malachite green by pandoraea pulmonicola YC32 using a batch and continuous system. *Journal of Hazardous Materials*, 172(2–3), 1439–1445. https://doi.org/10.1016/j.jhazmat.2009.08.009

Çetinkaya, H. F., Cebeci, M. S., Kaya, S., Jalbani, N. S., Maslov, M. M., & Marzouki, E. (2022). Removal of erythrosine B dye from wastewater using chitosan boric acid composite material: Experimental and density functional theory findings. *Journal of Physical Organic Chemistry*, e4400. https://doi.org/10.1002/poc.4400

Danouche, M., El Arroussi, H., Bahafid, W., & El Ghachtouli, N. (2021). An overview of the biosorption mechanism for the bioremediation of synthetic dyes using yeast cells. *Environmental Technology Reviews*, 10(1), 58–76. https://doi.org/10.1080/21622515.2020.1869839

Dennington, R., Keith, T. A., & Millam, J. M. (2016). *GaussView 6.0. 16*. Semichem Inc.

Dotto, G. L., & Pinto, L. A. A. (2011). Adsorption of food dyes acid blue 9 and food yellow 3 onto chitosan: Stirring rate effect in kinetics and mechanism. *Journal of Hazardous Materials*, 187(1–3), 164–170. https://doi.org/10.1016/j.jhazmat.2011.01.016

Gajera, H. P., Bambharolia, R. P., Darshna, H. G., Patel, S. V., & Golakiya, B. A. (2015). Molecular identification and characterization of novel Hypocrea koningii associated with azo dyes decolorization and biodegradation of textile dye effluents. *Process Safety and Environmental Protection*, 98, 406–416. https://doi.org/10.1016/j.psep.2015.10.005

Frisch, M. J., Trucks, G. W., Schlegel, H., Scuseria, G. E., Robb, M. A., Cheeseman, J. R., Scalmani, G., Barone, V., Petersson, G. A., Nakatsuji, H., Li, X., Caricato, M., Marenich, A. V., Bloino, J., Janesko, B. G., Gomperts, R., Mennucci, B., Hratchian, H. P., Ortiz, J. V., … Fox, D. J. (2009). *Gaussian 09, revision D.01*. Gaussian, Inc.

Fu, Y., & Viraraghavan, T. (2001). Fungal decolorization of dye wastewaters: A review. *Bioresource Technology*, 79(3), 251–262. https://doi.org/10.1016/s0960-8524(01)00028-1

Fu, Y., & Viraraghavan, T. (2000). Removal of a dye from an aqueous solution by the fungus aspergillus niger. *Water Quality Research Journal*, 35(1), 95–112. https://doi.org/10.2166/wqrj.2000.006

Fu, Y., & Viraraghavan, T. (2002). Decolorization and detoxification of Synozol red HF-6BN azo dye by Aspergillus niger and Nigrospora sp. *Advances in Environmental Research*, 7(1), 239–247. https://doi.org/10.1186/1735-2746-10-12

Hohenstein, E. G., Chill, S. T., & Sherrill, C. D. (2008). Assessment of the performance of the $M05 - 2X$ and $M06 - 2X$ exchange-correlation functionals for noncovalent interactions in biomolecules. *Journal of Chemical Theory and Computation*, 4(12), 1996–2000. https://doi.org/10.1021/ct800308k

Holzknecht, J., Dubrac, S., Hedtrich, S., Galgóczy, L., & Marx, F. (2022). Small, cationic antifungal proteins from filamentous fungi inhibit Candida albicans growth in 3D skin infection models. *Microbiology Spectrum*, 10(3), 00299–00222. https://doi.org/10.1128/spectrum.00299-22

Hu, T. L. (1996). Removal of reactive dyes from aqueous solution by different bacterial genera. *Water Science and Technology*, 34, 89–95. https://doi.org/10.1016/S0273-1223(96)00701-9

Huber, A., Hajdu, D., Khan, D. B., Gáspári, Z., Varbanov, M., Philippot, S., Fizil, A., Czajlik, A., Kele, Z., Sonderegger, C., Galgóczy, L., Bodor, A., Marx, F., & Batta, G. (2018). New antimicrobial potential and structural properties of PAFB: A cationic, cysteine-rich protein from Penicillium chrysogenum Q176. *Scientific Reports*, 8(1), 1751. https://doi.org/10.1038/s41598-018-20002-2

Kamal, S., Khalid, M., Khan, M. S., Shahid, M., & Ahmad, M. (2022). Amine-and imine-functionalized Mn-Based MOF as an unusual turn-on and turn-off sensor for d10 heavy metal ions and an efficient adsorbent to capture iodine. *Crystal Growth & Design*, 22(5), 3277–3294. https://doi.org/10.1021/acs.cgd.2c00092

Kamal, S., Khalid, M., Shahnawaz Khan, M., Shahid, M., Ashafaq, M., I, M., Shahwaz Ahmad, M., Ahmad, M., Faizan, M., & Ahmad, S. (2020). Synthesis, characterization and DFT studies of water stable Cd (II) metal–organic clusters with better adsorption property towards the organic pollutant in waste water. *Inorganica Chimica Acta*, 512, 119872. https://doi.org/10.1016/j.ica.2020.119872

Kamnev, A. A. (2013). Infrared spectroscopy in studying biofunctionalised gold nanoparticles. In *Nanomaterials imaging techniques, surface studies, and applications* (pp. 35–50). https://doi.org/10.1007/978-1-4614-7675-7-3

Kafa, A. H. T., Tüzün, G., Güney, E., Aslan, R., Sayın, K., Tüzün, B., & Ataseven, H. (2022). Synthesis, computational analyses, antibacterial and antibiofilm properties of nicotinamide derivatives. *Structural Chemistry*, 33(4), 1189–1197. https://doi.org/10.1007/s11224-022-01927-x

Kannan, C., Buvaneswari, N., & Palvannan, T. (2009). Removal of plant poisoning dyes by adsorption on tomato plant root and green carbon from aqueous solution and its recovery. *Desalination*, 249(3), 1132–1138. https://doi.org/10.1016/j.desal.2009.06.042

Kaur, M., & Datta, M. (2013). Adsorption equilibrium and kinetics of toxic dye-Erythrosine B adsorption onto montmorillonite. *Separation Science and Technology*, 48(9), 1370–1381. https://doi.org/10.1080/01496395.2012.727939

Kumar, R., & Ahmad, R. (2011). Biosorption of hazardous crystal violet dye from aqueous solution onto treated ginger waste (TGW). *Desalination*, 265(1–3), 112–118. https://doi.org/10.1016/j.desal.2010.07.040

Kunamneni, A., Ghazi, I., Camarero, S., Ballesteros, A., Plou, F. J., & Alcalde, M. (2008). Decolorization of synthetic dyes by laccase immobilized on epoxy-activated carriers. *Process Biochemistry*, 43(2), 169–178. https://doi.org/10.1016/j.procbio.2007.11.009

Lakhrissi, Y., Rbaa, M., Tuzun, B., Hichar, A., Anouar, E. H., Ounine, K., Almalki, F., Hadda, T. B., Zarrouk, A., & Lakhrissi, B. (2022). Synthesis, structural confirmation, antibacterial properties and bio-informatics computational analyses of new pyrrole based on 8-hydroxyquinoline. *Journal of Molecular Structure*, 1259, 132683. https://doi.org/10.1016/j.molstruc.2022.132683

Lecellier, A., Gaydou, V., Mounier, J., Hermet, A., Castrec, L., Barbier, G., Ablain, W., Manfait, M., Toubas, D., & Sockalingum, G. D. (2015). Implementation of an FTIR spectral library of 486 filamentous fungi strains for rapid identification of molds. *Food Microbiology*, 45(Pt A), 126–134. https://doi.org/10.1016/j.fm.2014.01.002

Li, Y., Zhao, R., Li, Y., & Zhou, Z. (2021). Limonin enhances the antifungal activity of eugenol nanoemulsion against Penicillium italicum in vitro and in vivo tests. *Microorganisms*, 9(5), 969. https://doi.org/10.3390/microorganisms9050969

Lozano, M., Rodríguez-Ulibarri, P., Echeverría, J. C., Beruete, M., Sorolla, M., & Beriain, M. J. (2017). Mid-infrared spectroscopy (MIR) for simultaneous determination of fat and protein content in meat of several animal species. *Food Analytical Methods*, 10(10), 3462–3470. https://doi.org/10.1007/s12161-017-0879-1

Malik, P. K., & Sanyal, S. K. (2004). Kinetics of decolourisation of azo dyes in wastewater by UV/H2O2 process. *Separation and Purification Technology*, 36(3), 167–175. https://doi.org/10.1016/S1383-5866(03)00212-0

Matos, A., Bezerra, R., & Dias, A. A. (2007). Screening of fungal isolates and properties of Ganoderma applanatum intended for olive mill wastewater decolorization and dephenolization. *Letters in Applied Microbiology*, 45(3), 270–275. https://doi.org/10.1111/j.1472-765X.2007.02181.x

Maurya, N. S., Mittal, A. K., Cornel, P., & Rother, E. (2006). Biosorption of dyes using dead macro fungi: effect of dye structure, ionic strength and pH. *Bioresource Technology*, 97(3), 512–521. https://doi.org/10.1016/j.biortech.2005.02.045

Mermer, A., Bulbul, M. V., Kalender, S. M., Keskin, I., Tuzun, B., & Eyupoglu, O. Y. (2022). Benzotriazole-oxadiazole hybrid compounds: Synthesis, anticancer activity, molecular docking and ADME profiling studies. *Journal of Molecular Liquids*, 359, 119264. https://doi.org/10.1016/j.molliq.2022.119264

Mittal, A., Mittal, J., Malviya, A., Kaur, D., & Gupta, V. K. (2010). Adsorption of hazardous dye crystal violet from wastewater by waste materials. *Journal of Colloid and İnterface Science*, 343(2), 463–473. https://doi.org/10.1016/j.jcis.2009.11.060

Nautiyal, P., Subramanian, K., & Dastidar, M. (2016). Adsorptive removal of dye using biochar derived from residual algae after in-situ transesterification: Alternate use of waste of biodiesel industry. *Journal of Environmental Management*, 182, 187–197. https://doi.org/10.1016/j.jenvman.2016.07.063

Okoye, C. C., Onukwuli, O. D., & Okey-Onyesolu, C. F. (2019). Utilization of salt activated Raphia hookeri seeds as biosorbent for Erythrosine B dye removal: Kinetics and thermodynamics studies. *Journal of King Saud University – Science*, 31(4), 849–858. https://doi.org/10.1016/j.jksus.2017.11.004

O'Mahony, T., Guibal, E., & Tobin, J. M. (2002). Reactive dye biosorption by Rhizopus arrhizus biomass. *Enzyme and Microbial Technology*, 31(4), 456–463. https://doi.org/10.1016/S0141-0229(02)00110-2

Pereira, L., & Alves, M. (2012). Dyes-environmental impact and remediation. In *Environmental protection strategies for sustainable development* (pp. 111–162). https://doi.org/10.1007/978-94-007-1591-2-4

Poustforoosh, A., Faramarz, S., Nematollahi, M. H., Hashemipour, H., Tüzün, B., Pardakhty, A., & Mehrabani, M. (2022). 3D-QSAR, molecular docking, molecular dynamics, and ADME/T analysis of marketed and newly designed flavonoids as inhibitors of Bcl-2 family proteins for targeting U-87 glioblastoma. *Journal of Cellular Biochemistry*, 123(2), 390–405. https://doi.org/10.1002/jcb.30178

Rashid, A., Bhatti, H. N., Iqbal, M., & Noreen, S. (2016). Fungal biomass composite with bentonite efficiency for nickel and zinc adsorption: A mechanistic study. *Ecological Engineering*, 91, 459–471. https://doi.org/10.1016/j.ecoleng.2016.03.014

Rezaeivala, M., Karimi, S., Sayin, K., & Tüzün, B. (2022). Experimental and theoretical investigation of corrosion inhibition effect of two piperazine-based ligands on carbon steel in acidic media. *Colloids and Surfaces A: Physicochemical and Engineering Aspects*, 641, 128538. https://doi.org/10.1016/j.colsurfa.2022.128538

Saeed, A., Iqbal, M., & Zafar, S. I. (2009). Immobilization of trichoderma viride for enhanced methylene blue biosorption: Batch and column studies. *Journal of Hazardous Materials*, 168(1), 406–415. https://doi.org/10.1016/j.jhazmat.2009.02.058

Salvi, N. A. (2018). Decolorization of Erythrosine B by Rhizopus arrhizus biomass. *Applied Water Science*, 8(7), 1–11. https://doi.org/10.1007/s13201-018-0800-0

Salvi, N. A., & Chattopadhyay, S. (2017). Biosorption of azo dyes by spent Rhizopus arrhizus biomass. *Applied Water Science*, 7(6), 3041–3054. https://doi.org/10.1007/s13201-016-0417-0

Saratale, R. G., Saratale, G. D., Chang, J. S., & Govindwar, S. P. (2011). Bacterial decolorization and degradation of azo dyes: A review. *Journal of the Taiwan Institute of Chemical Engineers*, 42(1), 138–157. https://doi.org/10.1016/j.jtice.2010.06.006

Schrödinger Release 2021-3. (2021a). *LigPrep*. Schrödinger.

Schrödinger Release 2021-3. (2021b). *Maestro*. Schrödinger.

Schrödinger Release 2021-3. (2021c). *QikProp*. Schrödinger.

Schrödinger Release 2019-4. (2019). Protein Preparation Wizard. Epik, Schrödinger, LLC, New York, NY, 2016; Impact, Schrödinger, LLC, New York, NY, 2016; Prime, Schrödinger, LLC, New York, NY.

Sharifzade, G., Asghari, A., & Rajabi, M. (2017). Highly effective adsorption of xanthene dyes (rhodamine B and erythrosine B) from aqueous solutions onto lemon citrus peel active carbon: Characterization, resolving analysis, optimization and mechanistic studies. *RSC Advances*, 7(9), 5362–5371. https://doi.org/10.1039/C6RA23157H

Singh, S., & Khajuria, R. (2018). Penicillium enzymes for the textile industry. In *New and future developments in microbial biotechnology and bioengineering*(pp. 201–215). https://doi.org/10.3390/membranes10110323

Smiciklas, I., Onjia, A., Raicevic, S., Janackovic, D., & Mitric, M. (2008). Factors influencing the removal of divalent cations by hydoxyapatite. *Journal of Hazardous Materials*, 152(2), 876–884. https://doi.org/10.1016/j.jhazmat.2007.07.056

Souza, F. H. M., Leme, V. F. C., Costa, G. O. B., Castro, K. C., Giraldi, T. R., Andrade, G., & S., S. (2020). Biosorption of rhodamine B using a low-cost biosorbent prepared from inactivated Aspergillus oryzae cells: Kinetic, equilibrium and thermodynamic studies. *Water, Air, & Soil Pollution*, 231(5), 242. https://doi.org/10.1007/s11270-020-04633-8

Şimşek, S., Kaya, S., Şenol, Z. M., Ulusoy, H. İ., Katin, K. P., Özer, A., Altunay, N., & Brahmia, A. (2022). Theoretical and experimental insights about the adsorption of uranyl ion on a new designed vermiculite-polymer composite. *Journal of Molecular Liquids*, 352, 118727. https://doi.org/10.1016/j.molliq.2022.118727

Taslimi, P., Kocyigit, U. M., Tüzün, B., & Kirici, M. (2022). Biological effects and molecular docking studies of Catechin 5-O-gallate: Antioxidant, anticholinergics, antiepileptic and antidiabetic potentials. *Journal of Biomolecular Structure & Dynamics*, 40(6), 2489–2497. https://doi.org/10.1080/07391102.2020.1840440

Tokalı, F. S., Taslimi, P., Demircioğlu, İ. H., Şendil, K., Tuzun, B., & Gülçin, İ. (2022). Novel phenolic Mannich base derivatives: Synthesis, bioactivity, molecular docking, and ADME-Tox studies. *Journal of the Iranian Chemical Society*, 19(2), 563–577. https://doi.org/10.1007/s13738-021-02331-8

Tonglairoum, P., Rojanarata, T., Ngawhirunpat, T., Akkaramongkolporn, P., Kaomongkolgit, R., & Opanasopit, P. (2017). Erythrosine incorporated fast-dissolving patches for dental plaque disclosing. *Advances in Pharmacology and Pharmacy*, 5(1), 12–19. https://doi.org/10.13189/app.2017.050102

Uysal, O. K., & Aral, E. C. (1998). Teratogenic effects and the role in the etiology of atopic diseases of erythrosine (FD and C Red No. 3). *Turkish Journal of Medical Sciences*, 28, 363–368.

Waghmode, T. R., Kurade, M. B., Kabra, A. N., & Govindwar, S. P. (2012). Degradation of remazol red dye by galactomyces geotrichum MTCC 1360 leading to increased iron uptake in sorghum vulgare and phaseolus mungo from soil. *Biotechnology and Bioprocess Engineering*, 17(1), 117–126. https://doi.org/10.1007/s12257-011-0307-0

Wang, X. S., Liu, X., Wen, L., Zhou, Y., Jiang, Y., & Li, Z. (2008). Comparison of basic dye crystal violet removal from aqueous solution by low-cost biosorbents. *Sepa. Separation Science and Technology*, 43(14), 3712–3731. https://doi.org/10.1080/01496390802222640

Wang, M. X., Zhang, Q. L., & Yao, S. J. (2015). A novel biosorbent formed of marine-derived Penicillium janthinellum mycelial pellets for removing dyes from dye-containing wastewater. *Chemical Engineering Journal*, 259, 837–844. https://doi.org/10.1016/j.cej.2014.08.003

Vautherin, D., & Brink, D. T. (1972). Hartree-Fock calculations with Skyrme's interaction. I. Spherical nuclei. *Physical Review C*, 5(3), 626–647. https://doi.org/10.1103/PhysRevC.5.626

Vijayaraghavan, K., & Yun, Y. S. (2008). Bacterial biosorbents and biosorption. *Biotechnology Advances*, 26(3), 266–291. https://doi.org/10.1016/j.biotechadv.2008.02.002

Vijayaraghavan, K., Mao, J., & Yun, Y. S. (2008). Biosorption ofmethylene blue fromaqueous solution using free and polysulfone-immobilized Corynebacterium glutamicum: Batch and column studies. *Bioresource Technology*, 99(8), 2864–2871. https://doi.org/10.1016/j.biortech.2007.06.008

Vimont, A., Fernandez, B., Ahmed, G., Fortin, H. P., & Fliss, I. (2019). Quantitative antifungal activity of reuterin against food isolates of yeasts and moulds and its potential application in yogurt. *International Journal of Food Microbiology*, 289(2019), 182–188. https://doi.org/10.1016/j.ijfoodmicro.2018.09.005

Yalazan, H., Tüzün, B., Akkaya, D., Barut, B., Kantekin, H., & Yıldırmış, S. (2022). Quinoline-fused both non-peripheral and peripheral ZnII and MgII phthalocyanines: Anti-cholinesterase, anti-α-glucosidase, DNA nuclease, antioxidant activities and in silico studies. *Applied Organometallic Chemistry*, 36(7), e6696. https://doi.org/10.1002/aoc.6696

Ye, M. P., Zhou, R., Shi, Y. R., Chen, H., & Du, C. Y. (2017). Effects of heating on the secondary structure of proteins in milk powders using mid-infrared spectroscopy. *Journal of Dairy Science*, 100(1), 89–95. https://doi.org/10.3168/jds.2016-11443

Yesilada, O., Cing, S., & Asma, D. (2002). Decolourisation of the textile dye astrazon red FBL by Funalia trogii pellets. *Bioresource Technology*, 81(2), 155–157. https://doi.org/10.1016/S0960-8524(01)00117-1

Zeroual, Y., Kim, B. S., Kim, C. S., Blaghen, M., & Lee, K. M. (2006). Biosorption of bromophenol blue from aqueous solutions by Rhizopus Stolonifer biomass. *Water, Air, and Soil Pollution*, 177(1–4), 135–146. https://doi.org/10.1007/s11270-006-9112-3